Unit Commitment Considering Static Voltage Stability through Worst-case Condition Detection

Jiaxin Wang
Dept. of Electrical Engineering
Tsinghua University
Beijing, China
jiaxinwangthu@gmail.com

Jiawei Zhang
Dept. of Electrical Engineering
Tsinghua University
Beijing, China
zhang-jw19@mails.tsinghua.edu.cn

Ning Zhang
Dept. of Electrical Engineering
Tsinghua University
Beijing, China
ningzhang@tsinghua.edu.cn

Goran Strbac
Dept. of Electrical Engineering
Imperial College London
London, UK
g.strbac@imperial.ac.uk

Fei Teng
Dept. of Electrical Engineering
Imperial College London
London, UK
f.teng@imperial.ac.uk

Yu Guo
Senior Planning Engineer
New York Independent System Operator
New York, USA
yguox@nyiso.com

2024 IEEE Power & Energy Society General Meeting (PESGM) | 979-8-3503-8183-2/24/$31.00 ©2024 IEEE | DOI: 10.1109/PESGM51994.2024.10688504

***Abstract*—Renewable intermittency and load fluctuations may lead to static voltage stability challenges in power systems. The power variation direction significantly influences the distance to saddle-node bifurcation (SNB). The worst-case variation direction corresponds to the shortest distance to SNB and is called the critical direction. In this paper, we propose a linear optimization model to determine the critical directions for power systems. Then, we integrate the direction into the unit commitment (UC) model, considering the static voltage stability requirements. Finally, we verify the method through five cases based on a modified IEEE 118-bus system. The results reflect the effectiveness of the critical direction determination and its application to UC. The UC results vary to safeguard the system's static voltage stability.**

***Index Terms*—static voltage stability, continuation power flow, worst-case scenarios, stability-constrained optimization.**

I. Introduction

THE voltage stability under the substantial integration of renewable poses a critical challenge for modern power systems. The renewable's intermittency can induce significant fluctuations in the system's net load [1]. These fluctuations may propel the system towards a saddle-node bifurcation (SNB) state, where the system voltage collapses [2]. In China, the installation of renewable has surpassed 1300 gigawatts, with this number continually rising. The escalating penetration of renewable is leading to an increasingly prevalent issue of static voltage instability. Consequently, there is a pressing need to prevent the system state from SNB and maintain an acceptable margin in the scheduling stage.

A crucial aspect in preventing the system from reaching SNB involves identifying the worst-case power variations. Varied directions result in different distances to SNB. The worst-case direction corresponds to the shortest distance to SNB and is called the critical direction. Unfortunately, determining the critical direction poses challenges. Initially, a heuristic method is proposed to calculate the critical direction [3]. This method requires iteratively solving a series of continuation power flow equations. Subsequently, a two-level (min-max) nonlinear optimization model is introduced to obtain the critical direction [4]. However, this model is non-convex and not solver-friendly. Besides, data-driven methods are popular in static voltage stability assessment. An ensemble oblique regression tree method is proposed to fit the stability margins by system operation states [5]. A physics-guided neural network is proposed to assess the stability margin online [6]. A transferable deep kernel emulator is proposed to assess the probability voltage margins [7]. Then, some model-driven methods are developed to model the voltage stability requirements in power system scheduling. A second-order cone programming is proposed to solve a voltage-stability-constrained optimal power flow [8]. A mixed integer second-order cone programming is proposed to solve a voltage-stability-constrained unit commitment [9]. These methods do not provide the corresponding critical direction and, thus, do not give an insight into the worst power variations.

We built a mixed-integer linear programming (MILP) model to solve the unit commitment (UC) problem considering static voltage stability. First, we derived an analytical formulation for the slope of the nose curve. Based on the derived formula, we proposed a linear optimization model to determine the critical direction d^*. Then, the maximum acceptable power variation amount λ^* is obtained. Finally, a UC with voltage stability requirements is built through the worst-case power variations $\lambda^* d^*$. Five cases are studied on a modified IEEE-118 system to demonstrate the effectiveness of the proposed model.

II. Critical Direction Determination

This section proposes a model-driven method to determine the worst-case power variation direction. First, an analytical formulation for the slope of the nose curve $V'(\lambda)$ is derived under a given direction d. Then, the tight relation between the

This work was supported by the National Natural Science Foundation of China (No. 52177093)

slope and the distance to SNB is revealed. Finally, a linear optimization model is built using the derived slope formula to find the critical direction.

A. Derivation of the Nose Curve's Slope

Suppose a power system with bus set $\mathcal{N}$ and branch set $\mathcal{E}$. Set $\mathcal{N}$ is composed of the set of generator buses $\mathcal{G}$, the set of renewable energy buses $\mathcal{R}$, and the set of load buses $\mathcal{L}$. The cardinality $|\cdot|$ of a set represents the number of elements in the set. The power flow equation is given by $f(\theta, V) = 0$, where $\theta \in \mathbb{R}^{|\mathcal{N}|-1}$ is the voltage angle vector, $V \in \mathbb{R}^{|\mathcal{N}|-|\mathcal{G}|}$ is the voltage magnitude vector, and $f(\cdot) \in \mathbb{R}^{2|\mathcal{N}|-|\mathcal{G}|-1}$ is the vector-valued function of the power flow. Given a direction of power injection variations $d \in \mathbb{R}^{2|\mathcal{N}|-|\mathcal{G}|-1}$, the power flow equation can be parameterized by a step size $\lambda \in \mathbb{R}$ as

$$g(\theta, V, \lambda) = f(\theta(\lambda), V(\lambda)) + \lambda d = 0. \tag{1}$$

Then, $V = V(\lambda)$ is called the nose curve under direction d, and the derivative $V'(\lambda)$ is the slope of the nose curve

$$\frac{\mathrm{d}\, V}{\mathrm{d}\, \lambda}(\theta, V) = \left[0, I_{|\mathcal{N}|-|\mathcal{G}|}\right] J_f(\theta, V)^{-1} \frac{\partial g}{\partial \lambda} = \tilde{D}(\theta, V) d, \tag{2}$$

where $I_{|\mathcal{N}|-|\mathcal{G}|}$ is the identity matrix of size $|\mathcal{N}| - |\mathcal{G}|$, $J_f(\theta, V)$ is the Jacobian matrix of $f(\theta, V)$, and $\tilde{D}(\theta, V) := \left[0, I_{|\mathcal{N}|-|\mathcal{G}|}\right] J_f(\theta, V)^{-1}$ for short. Although the direction d is predetermined, the coefficient matrix $\tilde{D}$ varies with the operating point (θ, V). Since $\tilde{D}$ has no analytical expression, the slope $V'(\lambda)$ cannot be calculated directly.

However, around the regular operating point, the coefficient matrix $\tilde{D}$ can be approximated by an analytical expression. Previous work [10] has shown that the power flow equation can be approximated as

$$\begin{cases} P_i \approx \sum_{(i,j)\in\mathcal{E}} \frac{1}{2} g_{ij}(V_i^2 - V_j^2) - b_{ij}(\theta_i - \theta_j) \\ Q_i \approx \sum_{(i,j)\in\mathcal{E}} -\frac{1}{2} b_{ij}(V_i^2 - V_j^2) - g_{ij}(\theta_i - \theta_j) \end{cases}, \tag{3}$$

which implies that

$$\tilde{D}(\theta, V) \approx \frac{1}{2} \operatorname{diag}^{-1}(V) D, \tag{4}$$

where $D \in \mathbb{R}^{(|\mathcal{N}|-|\mathcal{G}|)\times(2|\mathcal{N}|-|\mathcal{G}|-1)}$ is a constant matrix calculated from the admittance. Therefore, the slope can be approximated as

$$\frac{\mathrm{d}\, V}{\mathrm{d}\, \lambda} \approx \frac{1}{2} \operatorname{diag}^{-1}(V) D d < 0. \tag{5}$$

The negative sign is consistent with the fact that the upper part of the nose curve is stable.

B. Calculation of the Critical Direction

The distance to SNB is closely tied to the slope of the current operating state, as shown in Fig. 1. A steeper slope corresponds to a shorter distance. Hence, maximizing the derivative $V'(\lambda)$ can determine the critical direction. Moreover, the voltage component $\operatorname{diag}^{-1}(V)$ and the directional component Dd are decoupled. The per-unit value of the voltages around the regular operating point is close to one, while the directional part Dd signifies the degree of steepness.

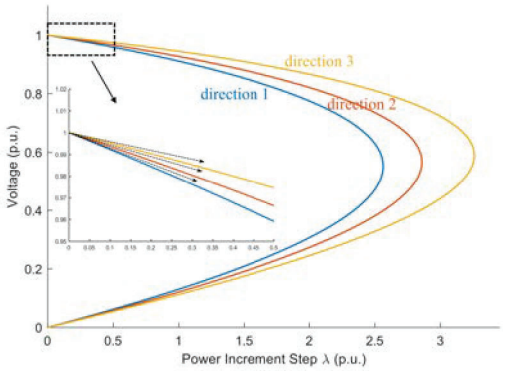

Fig. 1. The distance to SNB is closely tied to the slope of the current operating state. A steeper slope corresponds to a shorter distance.

A two-level linear optimization model (6) is proposed to calculate the critical direction. The direction d can be partitioned into three parts: the generator power injections $d_{\mathcal{G}}$, the load power injections $d_{\mathcal{L}}$, and the renewable power injections $d_{\mathcal{R}}$. Both $d_{\mathcal{L}}$ and $d_{\mathcal{R}}$ are further partitioned into the active power injections $d_{\mathcal{L},p}$ and $d_{\mathcal{R},p}$, and the reactive power injections $d_{\mathcal{L},q}$ and $d_{\mathcal{R},q}$, while $d_{\mathcal{G}}$ only includes the active power injections $d_{\mathcal{G},p}$. From the system operators' view, $d_{\mathcal{L}}$ and $d_{\mathcal{R}}$ are uncontrollable, while $d_{\mathcal{G}}$ is controllable. Thus, the inner level finds the optimal $d_{\mathcal{L}}$ and $d_{\mathcal{R}}$ such that the degree of the nose curve's steepness is maximized; the outer level finds the optimal $d_{\mathcal{G}}$ such that the degree of the nose curve's steepness is minimized.

$$\min_{d_{\mathcal{G}}} \max_{d_{\mathcal{L}}, d_{\mathcal{R}}} \quad \|Dd\|_1 = -1^{\mathrm{T}} Dd \tag{6a}$$

$$\text{s.t.} \quad d_{i,p} \geq 0, \forall i \in \mathcal{G} \tag{6b}$$

$$d_{j,p} \leq 0, \forall j \in \mathcal{L} \cup \mathcal{R} \tag{6c}$$

$$-q_j d_{j,p} \leq d_{j,q} \leq q_j d_{j,p}, \forall j \in \mathcal{L} \cup \mathcal{R} \tag{6d}$$

$$\sum_{i\in\mathcal{G}} d_{i,p} + \sum_{j\in\mathcal{L}} d_{j,p} + \sum_{k\in\mathcal{R}} d_{k,p} = 0, \tag{6e}$$

$$\sum_{i\in\mathcal{L}} d_{i,p} + \sum_{k\in\mathcal{R}} d_{k,p} = -1, \tag{6f}$$

$$d_{\mathcal{G}} := [(d_{i,p})_{i\in\mathcal{G}}], d_{\mathcal{L}} := [(d_{j,p}, d_{j,q})_{j\in\mathcal{L}}], \tag{6g}$$

$$d_{\mathcal{R}} := [(d_{k,p}, d_{k,q})_{j\in\mathcal{R}}], d := [d_{\mathcal{G}},\ d_{\mathcal{L}},\ d_{\mathcal{R}}]. \tag{6h}$$

The objective (6a) is to first maximize the norm of the directional components Dd over $d_{\mathcal{L}}$ and $d_{\mathcal{R}}$, and then minimize it over $d_{\mathcal{G}}$. The norm $\|Dd\|_1 = -1^{\mathrm{T}} Dd$ since Dd is a negative vector. Constraints (6b)-(6c) are the power injection constraints, where the positive sign refers to the positive injective power. Constraint (6d) is the power factor constraint, where q_j is a predetermined parameter. Constraint (6e) ensures the power balance. Constraint (6f) is a technical requirement to limit the total amount of injections. We point out that the sign of $d_{j,p}$ in (6c) can be changed according to practical requirements. This paper uses a negative sign since the rise in the net load worsens the static voltage stability.

Although problem (6) is a two-level optimization model, it

can be decoupled into two single optimization models. From the system operators' view, only the critical directions of load and renewable power injections $d_{\mathcal{L}}$ and $d_{\mathcal{R}}$ need to be identified due to their uncontrollability. Thus, the variables $d_{\mathcal{L}}$ and $d_{\mathcal{R}}$ are expected to be decoupled from $d_{\mathcal{G}}$. The three variables are coupled in constraint (6e). However, when combining with constraint (6f), the constraint (6e) can be equivalently replaced by

$$\sum_{i\in\mathcal{G}} d_{i,p} = -(\sum_{i\in\mathcal{L}} d_{i,p} + \sum_{k\in\mathcal{R}} d_{k,p}) = 1, \tag{7}$$

where the variables $d_{\mathcal{L}}, d_{\mathcal{R}}$ are decoupled from $d_{\mathcal{G}}$.

Hence, the critical direction can be determined by solving the single-layer linear optimization problem (8).

$$\min_{d_{\mathcal{L}}, d_{\mathcal{R}}} \quad 1^{\mathrm{T}}(D^{\mathcal{L}} d_{\mathcal{L}} + D^{\mathcal{R}} d_{\mathcal{R}}) \tag{8a}$$

$$\text{s.t.} \quad d_{j,p} \le 0, \forall j \in \mathcal{L}\cup\mathcal{R} \tag{8b}$$

$$-q_j d_{j,p} \le d_{j,q} \le q_j d_{j,p}, \forall j \in \mathcal{L}\cup\mathcal{R} \tag{8c}$$

$$\sum_{i\in\mathcal{L}} d_{i,p} + \sum_{k\in\mathcal{R}} d_{k,p} = -1, \tag{8d}$$

In the objective (8a), the coefficient matrix D is partitioned into $D = [D^{\mathcal{G}}, D^{\mathcal{L}}, D^{\mathcal{R}}]$ according to the partition of d. The final optimization model (8) is a single linear optimization, which can be solved efficiently by commercial solvers.

Although the determination model (6) and (8) only use the directional component Dd, the identified critical direction d^* is accurate. The reason is that the magnitude relationships among different buses' slopes stay consistent when voltage V varies from $V \approx 1$ to SNB. This magnitude relationship consistency is also verified by the numerical results in Section IV.

III. UC Considering Static Voltage Stability

This section presents a UC model considering the static voltage stability. First, the maximum acceptable power variations $\lambda^* d^*$ are identified. When the worst variations $\lambda^* d^*$ occur, the system is expected to be secure. Thus, a UC model with the voltage stability requirements is formulated.

A. Identifying the Maximum Acceptable Power Variations

This subsection identifies the maximum acceptable power variations $\lambda^* d^*$, or equivalently, the maximum acceptable increment step λ^*. The theoretical distance from the current operating point to SNB can be obtained straightforwardly because all the voltage magnitudes reach SNB simultaneously. However, before the system reaches SNB, the voltage magnitudes may have already dropped to an unacceptable level for many devices. λ^* is less than the distance to SNB.

To identity λ^*, there are three steps as follows.

1) Obtain the critical direction d^*: Solve the linear optimization problem (8) to obtain the critical direction $d^*_{\mathcal{L}}$ and $d^*_{\mathcal{R}}$. Then, substitute $d^*_{\mathcal{L}}$ and $d^*_{\mathcal{R}}$ into the two-level optimization problem (6), and solve the outer linear optimization problem to obtain the critical direction $d^*_{\mathcal{G}}$. We point out that the outer problem is also a decoupled single-layer optimization problem when $d^*_{\mathcal{L}}$ and $d^*_{\mathcal{R}}$ are obtained.

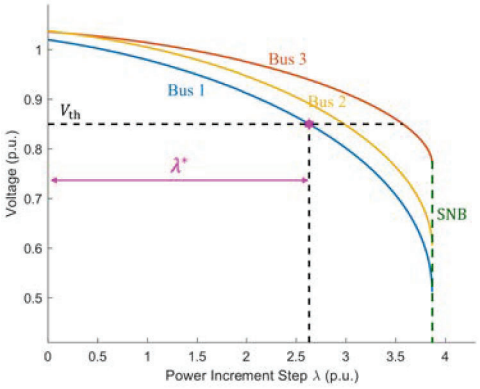

Fig. 2. Illustration of identifying the maximum acceptable power variations.

2) Simulate the nose curve $V = V(\lambda)$ along d^*: Calculate the system operation trajectory $V = V(\lambda)$ under critical direction d^* through continuation power flow. The continuation power flow is well-established. For example, the MATPOWER package provides a continuation power flow solver.

3) Evaluate λ^*: Given a voltage threshold V_{th} (e.g., 0.85 p.u.), the maximum acceptable increment step λ^* can be evaluated as

$$\lambda^* = \arg\max_{\lambda} \left\{ \lambda \;\middle|\; \min_{i\in\mathcal{N}} \{V_i(\lambda) \mid V_i'(\lambda) < 0\} \ge V_{\text{th}} \right\}. \tag{9}$$

Fig. 2 illustrates the process of identifying λ^*, which is represented by the magenta segment.

B. Unit Commitment With Voltage Stability Requirements

This subsection proposes a mixed-integer linear programming (MILP) model to solve the UC problem considering voltage stability requirements (UC-VSR) based on the maximum acceptable power variations $\lambda^* d^*$.

Let $\mathcal{U}$ be the set of unit commitment constraints. These constraints include minimum start-up and shut-down time, ramping, and power output constraints. Let $\mathcal{F}$ be the set of power flow equation constraints (3), and let $U = V^2$ be a new variable. Then, the proposed UC-VSR model is formulated as the following MILP problem (10), where all the variables with a tilde are the corresponding variables when the critical power variations $\lambda^* d^*$ occur.

The objective (10a) minimizes the total cost. Set $\mathcal{T}$ represents the time horizons. The first four terms are the generators' operation cost, where CF_g, CV_g, CSU_g, and CSD_g are the fixed cost, the variable cost, the start-up cost, and the shut-down cost, respectively. The binary variables $x_{g,t}$, $su_{g,t}$, and $sd_{g,t}$ indicate whether Generator g is on, started up, and shut down, respectively. The variable $P^{\mathcal{G}}_{g,t}$ is the active power output of Generator g. The last term is the additional start-up penalty cost caused by the power variations $\lambda^* d^*$. Constraints (10b) and (10h) are power flow equations, where $P_{i,t}, Q_{i,t}$ represent net nodal power injections, which are composed of the generators' output, the renewable's output, and the load's consumption, as shown in constraints (10c)-(10e) and (10j)-(10k). Constraints (10c) and (10i) are unit commitment

constraints. Equation (10f)-(10g) represents power variations $\lambda_t^* d^*$ occur in the load and renewable. These two constraints (marked in purple) coupled the two sets of decision variables, i.e., without-tilde variables under regular operation and with-tilde variables under critical operation. A traditional UC is required to calculate λ_t^*. In our practical tests, the iterations between λ_t^* and problem (10) are commonly unnecessary.

$$\min \sum_{g\in\mathcal{G},t\in\mathcal{T}}(\mathrm{CF}_g x_{g,t}+\mathrm{CV}_g P^{\mathcal{G}}_{g,t}+\mathrm{CSU}_g su_{g,t} +\mathrm{CSD}_g sd_{g,t}+\mathrm{CP}_g|\tilde{x}_{g,t}-x_{g,t}|) \tag{10a}$$

$$\text{s.t.}(\theta_{i,t},U_{i,t},P_{i,t},Q_{i,t})_{i\in\mathcal{N}}\in\mathcal{F},\forall t\in\mathcal{T} \tag{10b}$$

$$(P^{\mathcal{G}}_{g,t},Q^{\mathcal{G}}_{g,t},x_{g,t},su_{g,t},sd_{g,t})\in\mathcal{U},\forall g\in\mathcal{G},t\in\mathcal{T} \tag{10c}$$

$$P_{i,t}=P^{\mathcal{G}}_{g,t}-P^{\mathcal{L}}_{i,t}+P^{\mathcal{R}}_{r,t},\forall i\in\mathcal{N},t\in\mathcal{T} \tag{10d}$$

$$Q_{i,t}=Q^{\mathcal{G}}_{g,t}-Q^{\mathcal{L}}_{i,t}+Q^{\mathcal{R}}_{r,t},\forall i\in\mathcal{N},t\in\mathcal{T} \tag{10e}$$

$$[\widetilde{P^{\mathcal{L}}_{i,t}},\widetilde{Q^{\mathcal{L}}_{i,t}}]_{i\in\mathcal{L}}=[P^{\mathcal{L}}_{i,t},Q^{\mathcal{L}}_{i,t}]_{i\in\mathcal{L}}+\lambda_t^* d^*_{\mathcal{L}},\forall t\in\mathcal{T} \tag{10f}$$

$$[\widetilde{P^{\mathcal{R}}_{r,t}},\widetilde{Q^{\mathcal{R}}_{r,t}}]_{r\in\mathcal{R}}=[P^{\mathcal{R}}_{r,t},Q^{\mathcal{R}}_{r,t}]_{r\in\mathcal{R}}+\lambda_t^* d^*_{\mathcal{R}},\forall t\in\mathcal{T} \tag{10g}$$

$$(\widetilde{\theta_{i,t}},\widetilde{U_{i,t}},\widetilde{P_{i,t}},\widetilde{Q_{i,t}})_{i\in\mathcal{N}}\in\mathcal{F},\forall t\in\mathcal{T} \tag{10h}$$

$$(\widetilde{P^{\mathcal{G}}_{g,t}},\widetilde{Q^{\mathcal{G}}_{g,t}},\widetilde{x_{g,t}},\widetilde{su_{g,t}},\widetilde{sd_{g,t}})\in\mathcal{U},\forall g\in\mathcal{G},t\in\mathcal{T} \tag{10i}$$

$$\widetilde{P_{i,t}}=\widetilde{P^{\mathcal{G}}_{g,t}}-\widetilde{P^{\mathcal{L}}_{i,t}}+\widetilde{P^{\mathcal{R}}_{r,t}},\forall i\in\mathcal{N},t\in\mathcal{T} \tag{10j}$$

$$\widetilde{Q_{i,t}}=\widetilde{Q^{\mathcal{G}}_{g,t}}-\widetilde{Q^{\mathcal{L}}_{i,t}}+\widetilde{Q^{\mathcal{R}}_{r,t}},\forall i\in\mathcal{N},t\in\mathcal{T} \tag{10k}$$

IV. Case Studies

A. Data Description

A modified IEEE-118 system is used as the test system in this section. The system has 172 buses (including 118 load buses and 54 terminals), 240 transmission lines, 25 renewable energy sources, and 29 synchronous generators. The system is drawn in Fig. 3. Three types of synchronous generators (667 MW, 600 MW, 300 MW) are considered. The minimum on (off) time is 10 (18) hours, 10 (16) hours, and 4 (6) hours for the three types, respectively. The total load demand is 6040 MW on average. The total renewable energy capacity is 2500 MW, and the annual capacity utilization hour is 1854 on average. The base power is set as 100 MW.

The codes are finished in Matlab R2022b, Python 3.10, and Gurobi 10.0 and are executed on an AMD-RT-5950X CPU.

B. Critical Direction Results

The numerical results suggest that the slope $V'(\lambda)$ of the nose curve reflects the sensitivity to the power injection variations. Different buses have different slopes, corresponding to different sensitivities to the nodal power injections. Fig. 4 shows the slope $V'(\lambda)$ of the nose curve at each bus. From the figure, the top two buses with the largest slopes are Bus #150 and Bus #6. Bus #150 is a renewable bus, and Bus #6 is a load bus. These two buses are the weak buses of the system. The continuation power flow results shown in Fig. 5 also verify this conclusion. The voltage magnitudes of Bus #150 and Bus #6 decrease most rapidly when the power injections increase.

Three other directions, d^A, d^B, and d^C, are randomly generated to compare with the critical direction d^*. The

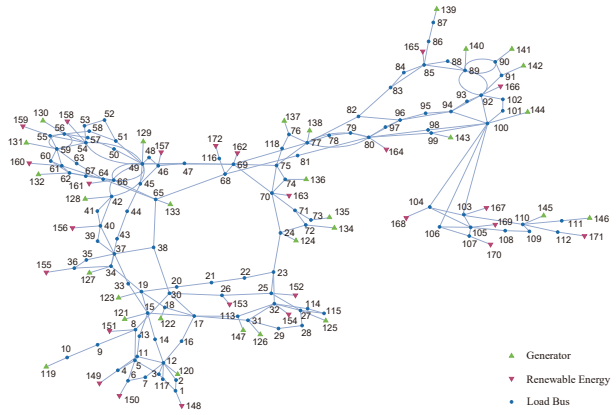

Fig. 3. IEEE-118 Network. The blue nodes represent buses, the green triangles represent generators, and the pink triangles represent renewable.

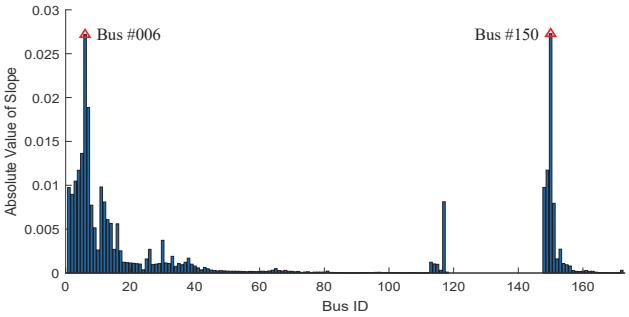

Fig. 4. Evaluation of the slopes $V'(\lambda)$ for all buses.

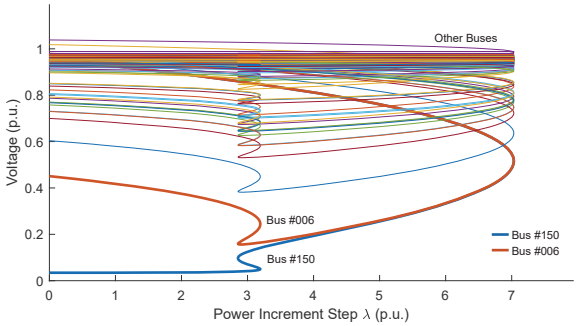

Fig. 5. Voltage trajectory $V=V(\lambda)$ along the critical direction d^*.

corresponding nose curves are shown in Fig. 6. The distance to SNB along direction d^A is $\lambda=42.0$, along direction d^B is $\lambda=26.6$, along direction d^C is $\lambda=100.7$, while along the critical direction d^* is only $\lambda=7.0$. The results suggest that the critical direction d^* obtained by the proposed model can reflect the most sensitive direction to the power variations.

For large-scale systems, the proposed approach is efficient. It costs 3 seconds for a Polish system with 2383 buses, and costs 120 seconds for a European system with 9241 buses. Both systems can be found in MATPOWER.

C. UC-VSR Scheduling Results

A 48-horizon UC-VSR scheduling problem is built based on the modified IEEE-118 system.

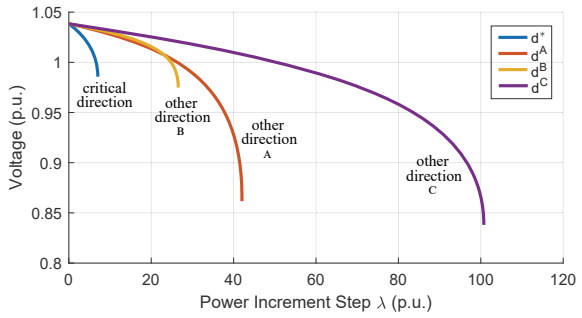

Fig. 6. Comparison of the distance to SNB along different directions. The critical direction d^* corresponds to the shortest.

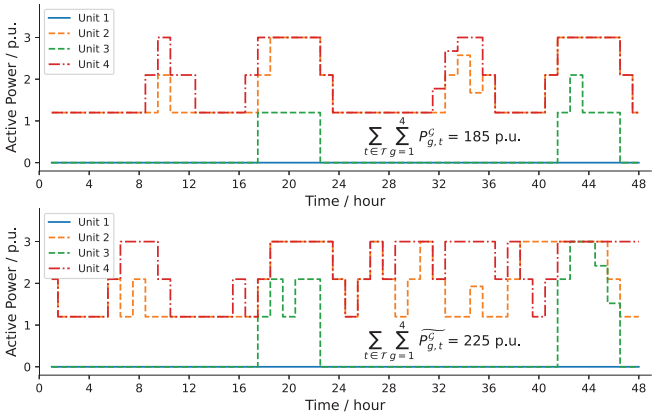

Fig. 7. Active power output of four generators that are the top four closest to the identified weak buses.

Fig. 7 shows the active power output of four generators that are the top four closest to the identified weak buses, Bus #150 and Bus #6. The four generators are connected at Bus #119, Bus #120, Bus #121, and Bus #122, respectively. The upper figure shows the power curve $P^{\mathcal{G}}_{g,t}$ corresponding to the regular condition, and the lower figure shows the power curve $\widetilde{P^{\mathcal{G}}_{g,t}}$ corresponding to the critical condition with $\lambda^* d^*$ variations. The results suggest that these close generators' power output is upward adjusted to support the static voltage stability around the weak buses. The total amount of these generators' power is increased from 185 p.u. to 225 p.u.. This accounts for 27.9% of the total incremental power of all generators, while the total capacity of these generators is only 8.8% of the total capacity of all generators. The results suggest that the proposed UC-VSR model can actively adjust power injections of generators close to weak buses to support voltage stability.

Five comparison cases with different load and renewable conditions are considered to compare the proposed UC-VSR model with the traditional UC model. The comparison results are shown in Table I. The UC-VSR model gives a secure scheduling result in all five cases that can immediately cope with the maximum acceptable power injection variations. The table shows that the UC-VSR model pays an additional 0.48% cost on average to ensure static voltage stability. The additional cost is mainly caused by the additional on-status units. As for the distance to SNB, 574.92 MW on average is reserved by the UC-VSR model, which is 6.64% larger than that of the UC model. Moreover, all the distance under critical conditions is reserved above 200 MW, giving a secure margin from SNB.

TABLE I
COMPARISON WITH TRADITIONAL UC

No.	Problem	Online Units[1]	Cost / kRMB	Margin[2]/ MW
1	UC	18.3	27741.7	540.6
	UC-VSR	18.9	27866.8	555.7
2	UC	15.9	26551.5	516.8
	UC-VSR	18.0	26790.2	583.5
3	UC	17.9	28457.8	553.8
	UC-VSR	18.1	28561.3	559.9
4	UC	16.3	29098.7	558.3
	UC-VSR	17.0	29214.7	561.1
5	UC	14.9	26060.3	526.0
	UC-VSR	15.6	26139.3	614.4

[1] Average number of online units in the 48-horizon scheduling. $|T|^{-1}\sum_{t\in\mathcal{T}}\sum_{g\in\mathcal{G}} x_{g,t}$ or $|T|^{-1}\sum_{t\in\mathcal{T}}\sum_{g\in\mathcal{G}} \widetilde{x}_{g,t}$.
[2] Average distance to SNB in the 48-horizon scheduling.

V. Conclusions

This paper proposed a linear optimization model to determine the critical direction, which reveals the worst-case power variations and weak buses. Then, a UC model considering static voltage stability was built, which incurs a minimal additional cost while safeguarding the stability. Numerical results on a modified IEEE-118 system verified the effectiveness of the proposed model.

References

[1] G. Pierrou and X. Wang, "Analytical study of the impacts of stochastic load fluctuation on the dynamic voltage stability margin using bifurcation theory," *IEEE Transactions on Circuits and Systems I: Regular Papers*, vol. 67, no. 4, pp. 1286–1295, 2020.

[2] X.-H. Zhao and H.-D. Chiang, "On the load margins and bifurcations of power system using quasi-steady state model," in *2017 IEEE Power & Energy Society General Meeting*, 2017, pp. 1–5.

[3] P. Kundur, *Power system stability and control*. McGraw-hill, Inc., 2007.

[4] L. S. Neves and L. F. Costa Alberto, "On the computation of the locally closest bifurcation point considering loading uncertainties and reactive power limits," *IEEE Transactions on Power Systems*, vol. 35, no. 5, pp. 3885–3894, 2020.

[5] H. Jia, Q. Hou, P. Yong, Y. Liu, N. Zhang, D. Liu, and M. Hou, "Voltage stability constrained operation optimization: an ensemble sparse oblique regression tree method," *IEEE Transactions on Power Systems*, pp. 1–13, 2023.

[6] M. E. C. Bento, "Physics-guided neural network for load margin assessment of power systems," *IEEE Transactions on Power Systems*, pp. 1–12, 2023.

[7] B. Tan, J. Zhao, and L. Xie, "Transferable deep kernel emulator for probabilistic load margin assessment with topology changes, uncertain renewable generations and loads," *IEEE Transactions on Power Systems*, vol. 38, no. 6, pp. 5740–5754, 2023.

[8] B. Cui and X. A. Sun, "A new voltage stability-constrained optimal power-flow model: Sufficient condition, socp representation, and relaxation," *IEEE Transactions on Power Systems*, vol. 33, no. 5, pp. 5092–5102, 2018.

[9] Z. Chu and F. Teng, "Voltage stability constrained unit commitment in power systems with high penetration of inverter-based generators," *IEEE Transactions on Power Systems*, vol. 38, no. 2, pp. 1572–1582, 2023.

[10] Z. Yang, H. Zhong, A. Bose, T. Zheng, Q. Xia, and C. Kang, "A linearized OPF model with reactive power and voltage magnitude: A pathway to improve the MW-only DC OPF," *IEEE Transactions on Power Systems*, vol. 33, no. 2, pp. 1734–1745, Mar. 2018.